 Water Supply | in press | 2021

Spatial-temporal pattern study on water conservation function using the SWAT model

Zhiyin Wang and Jiansheng Cao

ABSTRACT

The performance of the water conservation function (WCF) affects the water supply and flood control capabilities of an ecosystem. In this study, we combined the water balance method with the Soil and Water Assessment Tool (SWAT) model to calculate the water conservation amount (WCF) upstream of the Xiong'an New Area (Zijingguan-ZJG, Zhongtangmei-ZTM, and Fuping-FP basins) at annual and monthly scales from 2007 to 2017 and used multiple linear regression and geographic detector models to analyze the factors affecting the temporal changes and spatial pattern of the water conservation amount (WCA). Our results reveal that the annual WCAs of the ZTM basin are all positive, while the WCAs of the ZJG and FP basins have negative values in drought years. The annual WCAs in the upstream of each basin have changed between positive and negative values. On the monthly scale, all areas of the ZJG, ZTM, and FP basins have positive and negative value conversions of WCA between the rainy and non-rainy seasons. Precipitation, evapotranspiration, and their combined effects are the main factors leading to the temporal changes and spatial patterns of WCA in the study area. The above results can provide reference cases for other regions to carry out relevant research work.

Key words | geographic detector, multi-temporal scale, SWAT, water conservation function

Zhiyin Wang
University of Chinese Academy of Sciences,
Beijing 100049,
China

Jiansheng Cao (corresponding author)
Center for Agricultural Resources Research,
Institute of Genetics and Developmental Biology,
Chinese Academy of Sciences/Hebei Key Laboratory of Soil Ecology/Key Laboratory of Agricultural Water Resources,
Shijiazhuang 050022,
China
E-mail: *caojs@sjziam.ac.cn*

HIGHLIGHTS

- The combination of the SWAT model and water balance method can quantitatively calculate water conservation amount (WCA) on multi-temporal scales.
- The WCA has a positive-negative conversion of between rainy season and non-rainy season.
- Precipitation, evapotranspiration, and their combined effects are the main factors leading to the temporal changes and spatial pattern of WCA.

INTRODUCTION

Water resources are an essential fundamental resource for the sustainable development of agriculture, society, and economy in any region (Cao *et al.* 2020; Immerzeel *et al.* 2020). The water conservation function (WCF) is an essential function of the ecosystem to maintain water resources, including natural processes such as atmosphere, water, vegetation, and soil (Kurihara *et al.* 2018). The manifestations of the WCF mainly include the flood retention and runoff regulation of the ecosystem. Flood retention means that the ecosystem intercepts part of the rainwater through the forest canopy, litter layer, and soil layer of the

doi: 10.2166/ws.2021.127

vegetation, reducing the direct fall of precipitation on the surface, thereby significantly reducing the probability of flooding (Zhou *et al.* 2010; Návar 2017). Runoff regulation means that the ecosystem stores rainfall in the rainy season and replenishes the river in the dry season, thereby stabilizing the river's flow in the dry season. The role of WCF in flood interception and runoff regulation are different manifestations of WCF at different time scales. The evaluation of WCF is usually represented in terms of water conservation amount (WCA). The calculation methods of WCA mainly include the canopy interception method (Davies-Barnard *et al.* 2014), comprehensive water storage method (Liu *et al.* 2016), and water balance method (Scordo *et al.* 2018).The water balance method is the basis for studying the mechanism of water conservation, and the calculation results are more credible than other methods. It is currently the most commonly used and most extensive method in the quantitative study of WCFs. The water balance method regards the ecosystem as a complex, and from the perspective of water balance, the difference between precipitation and evapotranspiration and other consumption is considered the WCA (Ding *et al.* 2017). In the current research, the water balance method and the ecohydrological model are usually combined to carry out quantitative analyses on WCF at the basin scale.

Affected by topography, climate, soil, vegetation, and other factors at different time and space scales, the WCF has a significant time scale effect and regional differentiation effect (Wang *et al.* 2013). Different regions and different time and space scales may contain completely different manifestations of WCFs. Therefore, a multi-time scale study of the spatiotemporal changes of WCF can comprehensively evaluate the ecosystem's WCF. Most current studies use the average runoff over many years to calibrate model parameters (Cong *et al.* 2020; Xu *et al.* 2020). However, these studies can neither reflect the inter-annual changes in the WCF, let alone the intra-year changes in the WCF. Spatial stratified heterogeneity is one of the fundamental characteristics of geographic phenomena. At present, most studies on the factors affecting the spatial differentiation of WCFs are the correlation or principal component analysis between WCA and climate, human activities, and other factors, and there is a lack of quantitative analysis of the influencing factors (Luo *et al.* 2019).

As an indispensable tool for understanding the interaction between hydrological processes and the ecological environment, the SWAT eco-hydrological model has been widely used in ecohydrological research at the basin scale (Yang *et al.* 2018). The SWAT model can accurately simulate the hydrological cycle's physical processes, such as interception, surface runoff, evapotranspiration, infiltration, and underground runoff from time scales such as yearly, monthly, and daily through the division of hydrological response units and sub-basins. Simultaneously, it can reflect the unevenness of precipitation, evapotranspiration, and spatial distribution of the underlying surface. Combining the SWAT model with the water balance method can provide a new way for the multi-time scale study of spatiotemporal WCF changes. Geographic detector is a new spatial analysis model with an exact physical meaning that detects the spatial differentiation of geographic elements and reveals the influencing factors (Wang & Hu 2012). Geographic detector can not only quantitatively analyze the weight of each factor but also analyze the interaction between multiple factors.

On April 1, 2017, China's Central Committee and State Council decided to establish the Xiong'an New Area to build a green, ecological, and livable city. The upstream of Xiong'an New Area is the most crucial WCF area and ecological environment support area of Xiong'an New Area (Yang *et al.* 2018). The water conservation capacity of the ecosystem in the upstream basin dramatically affects the water supply and flood control safety of Xiong'an New Area. In this study, we take the upstream of Xiong'an New Area as the research area. Based on the basin SWAT model's construction, we combine the SWAT model with the water balance method to calculate the WCA at annual and monthly scales and analyze its temporal and spatial changes. Simultaneously, multiple linear regression and geographic detector models are used to study the influencing factors of WCA's temporal change and the influencing factors of WCA's spatial pattern. This study can provide a theoretical basis for decision-makers to formulate and adjust the upstream water resources management policy and ecological environment protection policy in the upstream of Xiong'an New Area.

MATERIALS AND METHODS

Overview of the study area

The study area is located in northern China's mountainous areas (38° 46′ 31″ ~ 39° 40′ 8″ N, 113° 40′ 4″ ~ 115° 10′1″ E), and includes three basins in the upstream of Xiong'an New Area, Zijingguan (ZJG), Zhongtangmei (ZJG) and Fuping (FP) basins, with a total area of 7,310.27 km^2 (Figure 1). The whole area's altitude is 149 to 2,611 m, gradually decreasing from northwest to southeast,and the main landform types are mountains and hills. The study area is located in a temperate monsoon climate zone, with hot and rainy summers, cold and dry winters, with an average annual temperature ranging from 7.4 to 12.8 °C and precipitation between 550 and 790 mm (Cui *et al.* 2019). Affected by the monsoon climate, the annual precipitation in the study area is uneven. Nearly 80% of the precipitation is concentrated in the rainy season from June to September (Zhao *et al.* 2012).

Data sources

The data used in this study include meteorological data, such as precipitation and temperature, surface runoff data, a digital elevation model (DEM), land use, soil type, and other spatial data. The resolution, time, and sources of socio-economic data such as gross domestic product (GDP) (10^4 yuan/km^2) and population density (persons/km^2) are shown in Table 1. The soil's hydrological properties are calculated based on the soil water characteristic software SPAW (Soil Plant Atmosphere Water) developed by the United States Department of Agriculture. The locations of four meteorological stations and the 42 evenly distributed precipitation stations are shown in Figure 1.

Construction of the SWAT model

The SWAT model divides the basin into multiple sub-basins according to the river network and water system, completes

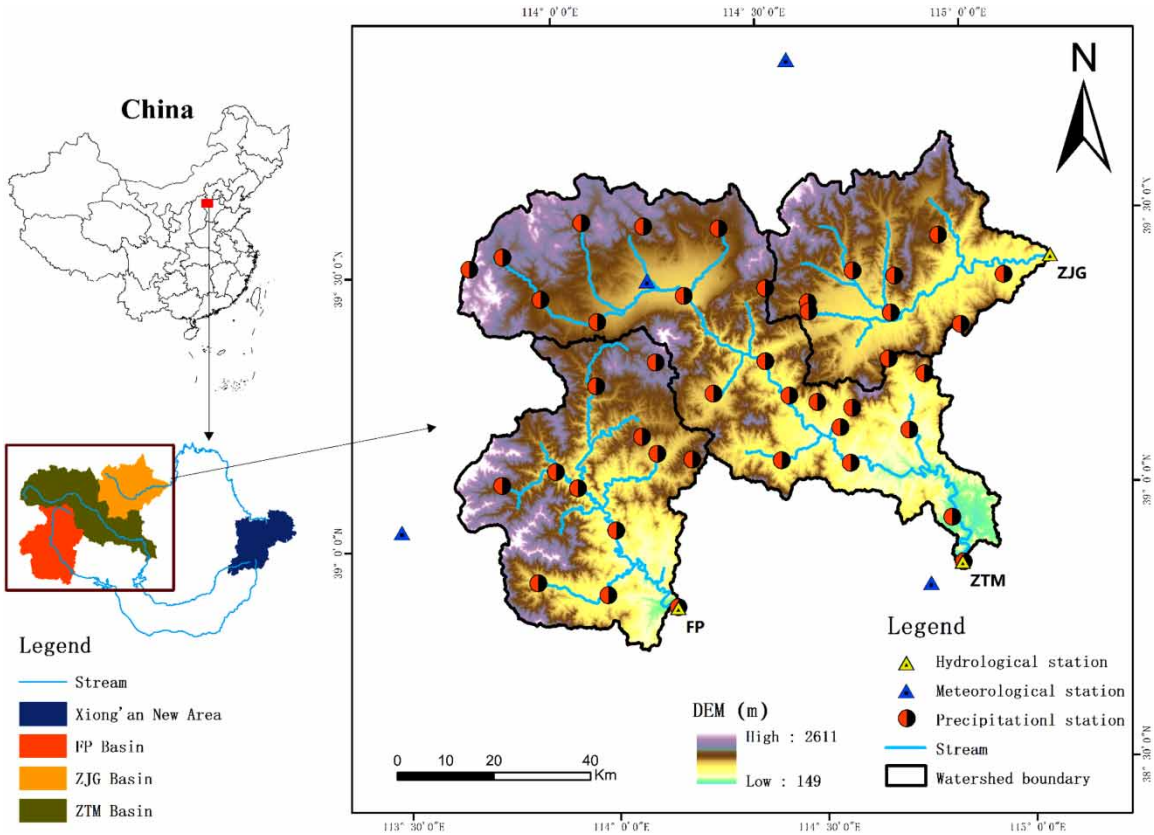

Figure 1 | Locations of the study area and hydrological gauging stations. (ZJG: Zijingguan; ZTM: Zhongtangmei; FP: Fuping).

Table 1 | The detailed information for data used in the study

Data	Resolution	Period	Source
Precipitation	Daily	2006–2017	The hydrological yearbook of Haihe River basin of China, collected by Haihe River Conservancy Commission.
Other meteorological factors	Daily	2006–2017	The National Climate Center of China Meteorological Administration (http://data.cma.cn/)
Runoff	Daily	2006–2017	The hydrological yearbook of Haihe River basin of China, collected by Haihe River Conservancy Commission.
Land-use map	100 m	2010	The Resource and Environmental Science Data Center of the Chinese Academy of Sciences (http://www.resdc.cn/)
Soil-type map	1 km	2010	The Cold and Arid Region Scientific Data Center of the Chinese Academy of Sciences (http://data.casnw.net/portal/)
DEM	30 m	2010	The International Scientific Data Service Platform of the Chinese Academy of Sciences (http://www.gscloud.cn/)
GDP map	1 km	2010	The Global Change Research Data Publishing & Repository (http://www.geodoi.ac.cn/)
Population density map	1 km	2007–2017	The East View Cartographic (https://www.satpalda.com/)

topological connections based on paths such as rivers, and then divides the sub-basins into smaller hydrological response units based on features such as surface cover, soil, and slope (Moriasi *et al.* 2007). The SWAT model used the Hydrological Response Unit (HRU) as the minimum simulation unit to simulate hydrological cycle processes. Previous research has shown that setting the area threshold of land use, soil, and slope to 0 can make the generated HRU reflect the actual amount and spatial distribution of land use (Kan *et al.* 2017).

In the SWAT model construction of this study, the surface runoff, the surface runoff was calculated using the soil conservation service (SCS) runoff curve model, the soil water content simulation was using the dynamic water storage reservoir model, the reference evapotranspiration calculation was using the Penman-Monteith formula, and the groundwater runoff was calculated using the basal flow regression coefficient method (Han *et al.* 2012).

SWAT-CUP is a calibration software specially developed by the Swiss Federal Institute of Water Quality Science and Technology for the SWAT model (Khatun *et al.* 2018). The software realizes automatic parameter calibration and can give the optimal parameter value and the optimal parameter value range. The SUFI-2 algorithm in SWAT-CUP software is a common method for uncertainty analysis of hydrological models (Cao *et al.* 2018). The SUFI-2 algorithm takes into account uncertain sources such as model structure, monitoring data, model parameters. Therefore, this paper intends to select the SUFI-2 method for watershed parameter calibration. The simulation results were evaluated using the Nash-Sutcliffe (NSE) (Nash & Sutcliffe 1970), correlation coefficient (R^2) (Zuo *et al.* 2016), and relative bias (PBIAS) (van Griensven *et al.* 2006). The model parameters and simulation results have been published in Forests (Wang *et al.* 2021). The results of model calibration and verification are shown in Table 2.

The calculation method of WCA based on the SWAT model

Using the water balance method to calculate WCA takes the difference between precipitation and evapotranspiration and other consumption as WCA. The equation is as follows:

$$W = P - AET - R \tag{1}$$

where W is the water conservation amount; P, AET, and R are precipitation, actual evapotranspiration, and surface runoff, respectively.

The water balance equation based on the SWAT model can be expressed as:

$$\Delta S_i = PREC_i - AET_i - WYLD_i \tag{2}$$

$$WYLD_i = SURQ_i + LATQ_i + GWQ_i \tag{3}$$

Table 2 | Calibration and validation for annual and monthly runoff for three basins

		Calibration period (2007–2012)			Validation period (2013–2017)		
Time Scale	**Hydrological Station**	**NSE**	**R^2**	**PBIAS (%)**	**NSE**	**R^2**	**PBIAS (%)**
Year	ZJG	0.87	0.92	−2.13	0.88	0.90	5.10
	ZTM	0.86	0.90	1.54	0.85	0.88	8.43
	FP	0.89	0.90	0.84	0.87	0.89	3.30
Month	ZJG	0.83	0.87	10.81	0.82	0.84	5.77
	ZTM	0.84	0.86	8.75	0.80	0.85	8.40
	FP	0.82	0.87	−1.93	0.81	0.85	4.59

where ΔS_i represents the amount of water change on the ith HRU; $PREC_i$ represents the precipitation of the ith HRU; AET_i represents the actual evapotranspiration of the ith HRU; $WYLD_i$ represents the total runoff from the ith HRU, $WYLD_i$ includes surface runoff $SURQ_i$, Soil flow $LATQ_i$, underground runoff GWQ_i.

According to the definition of formula (1), the WCA Y_i of the ith HRU can be expressed as:

$$W_{ij} = PREC_{ij} - AET_{ij} - SURQ_{ij} \tag{4}$$

where W_{ij} is the water conservation amount of the ith HRU (mm); $PREC_i$ represents the rainfall of the ith HRU (mm); AET_{ij} represents the actual evapotranspiration of the ith HRU (mm); $SURQ_{ij}$ represents the surface runoff produced by the ith HRU (mm) and j represents the value corresponding to the year and month time scales.

Analysis of influencing factors based on geographic detectors

The geographic detector has the advantage of simultaneously detecting the different influences and interactions of multiple factors in different spatial units (Jin-Feng *et al.* 2009; Wang *et al.* 2010). This study mainly uses factor detection and interactive detection modules to quantitatively analyze the influencing factors and their interactions of the spatial variability of water conservation functions in the river basin. The calculation model is as follows:

$$q = 1 - \frac{\sum_{h=1}^{L} N_h \sigma_h^2}{N\sigma^2} = 1 - \frac{SSW}{SST} \tag{5}$$

in which

$$SSW = \sum_{h=1}^{L} N_h \sigma_h^2,\ SST = N\sigma^2 \tag{6}$$

where q represents the detection force value of the impact factor on WCA, and the range of the domain value is [0, 1]. The higher the value is, the more significant the impact of classification factors on WCA is; $h = 1, \ldots,$ L is the stratification of variable Y or factor X, namely classification or partition; N_h and N are the number of units in layer h and the whole area, respectively; σ_h^2 and σ^2 are the Y values variances for layer H and the whole region, respectively. SSW and SST are within the sum of squares and the total sum of squares, respectively.

In this study, we first used the Acrgis 10.1 to perform spatial overlay analysis on the WCA layer and impact factor layer in 2010, and reclassified the factors to obtain type variables. The value of the dependent variable Y is a numerical quantity, representing the area attribute of each WCA patch. The independent variables X1, X2, …, X8 are type quantity, which is respectively the categorical attribute values of precipitation, potential evapotranspiration, altitude, slope, soil type, land use, GDP, and population density. We bring the X and Y data into the geographic detector model to get the q value result, and finally get the maximum q value by adjusting the classification criteria of the independent variable X. The value range of q is [0–1]. The larger the value, the stronger the explanatory power of this factor to the Y value (Todorova *et al.* 2016).

With the aid of the interactive detector module of the geographic detector, we evaluate whether the two impact factors will increase or decrease the explanatory power of

the independent variable X to the dependent variable Y when they work together. The larger the value, the more it means that the two impact factors have a more significant effect on Y than a single impact factor.

RESULTS

Spatio-temporal changes of WCA

Annual conservation amount

It can be seen from Figure 2 that the inter-annual variation of WCA in the ZJG, ZTM, and FP basins was considerable. The multi-year average value of WCA was the largest in the ZJG basin, which was 47.59 mm, and the smallest was the FP basin, which was 4.55 mm. The maximum WCA in ZJG, ZTM, and ZTM basins all appeared in 2011, and the values were 47.59 mm, 103.88 mm, and 49.26 mm, respectively. At this time, most regions of the study area were positive regions of WCA. The high positive value regions of WCA mainly appeared in the ZJG basin and the middle and lower reaches of the ZTM basin; the moderate positive value regions of WCA mainly appeared in the southwest of the FP basin; the low positive value regions of WCA mainly appeared in the upstream area of the ZTM basin (Figure 3(e)).The minimum values of WCA in the ZJG and FP basins were all negative, and the values were −8.4 mm in 2014 and −55.65 mm in 2017, respectively. In 2014, most of the ZJG basin was the low positive value region of WCA. In the upstream of the ZJG basin, the sub-basins 5, 8, and 10 showed the moderate negative value region of WCA, while the sub-basin 7 showed the high negative value region of WCA (Figure 3(h)). In 2017, the FP basins were all areas with negative WCA, and the middle and lower reaches of the FP basin were dominated by the moderate and high negative value region of WCA (Figure 3(k)). The minimum value of WCA in the ZTM basin was positive, which was 1.86 mm in 2009. At this time, the upstream of the ZTM basin was mainly the moderate positive value region of WCA, while the upstream of the ZTM basin was mainly the low and moderate negative value region of WCA. Furthermore, the low positive value region of WCA showed in sub-basins 2, 3, 4, 7, 12, and 14 (Figure 3(c)).

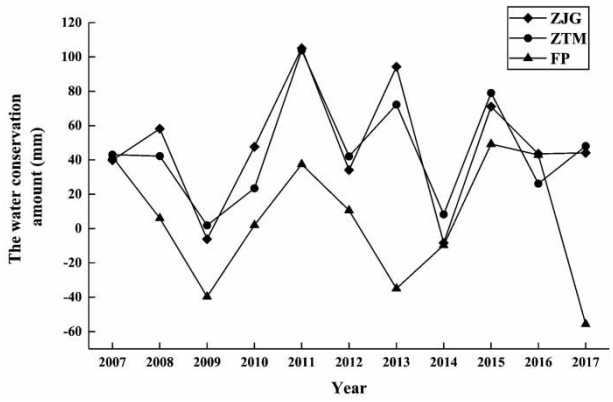

Figure 2 | Interannual variation of WCA in the three basins.

Monthly conservation amount

It can be seen from Figure 4 that there were apparent differences in WCA in different months in each basin, which was not only reflected in the magnitude but also positive and negative changes. A negative WCA indicated that the WCA in the month was at a loss. The variability of WCA in the ZJG and ZTM basins was the largest in July, and the variability of WCA in the FP basin was the largest in August. The WCA in the rainy season (June-September) of each basin was positive, while the WCA in the non-rainy season (October-May) was negative.

The WCA of the ZJG, ZTM, and FP basins all reached their maximum in July, with values of 32.12 mm, 28.87 mm, and 37.18 mm, respectively (Figure 4). At this time, the study areas were all positive value regions of WCA, and the high positive value regions of WCA mainly appeared in the lower reaches of each basin. The moderate positive value regions of WCA mainly appeared in the upper reaches of the ZJG basin, the middle reaches of the ZTM basin, and the middle and upper reaches of the FP basin. The low positive value regions of WCA mainly appeared in the upper reaches of the ZTM basin (Figure 5(g)). The lowest values of WCA in ZJG, ZTM, and FP basins were all negative values. The lowest WCA values in the ZJG basin and FP basin occurred in November and October, respectively, with values of −8.61 mm and −17.89 mm, respectively. In November, the ZJG basin was dominated by the moderate and low negative value regions of WCA, and the high negative value regions of

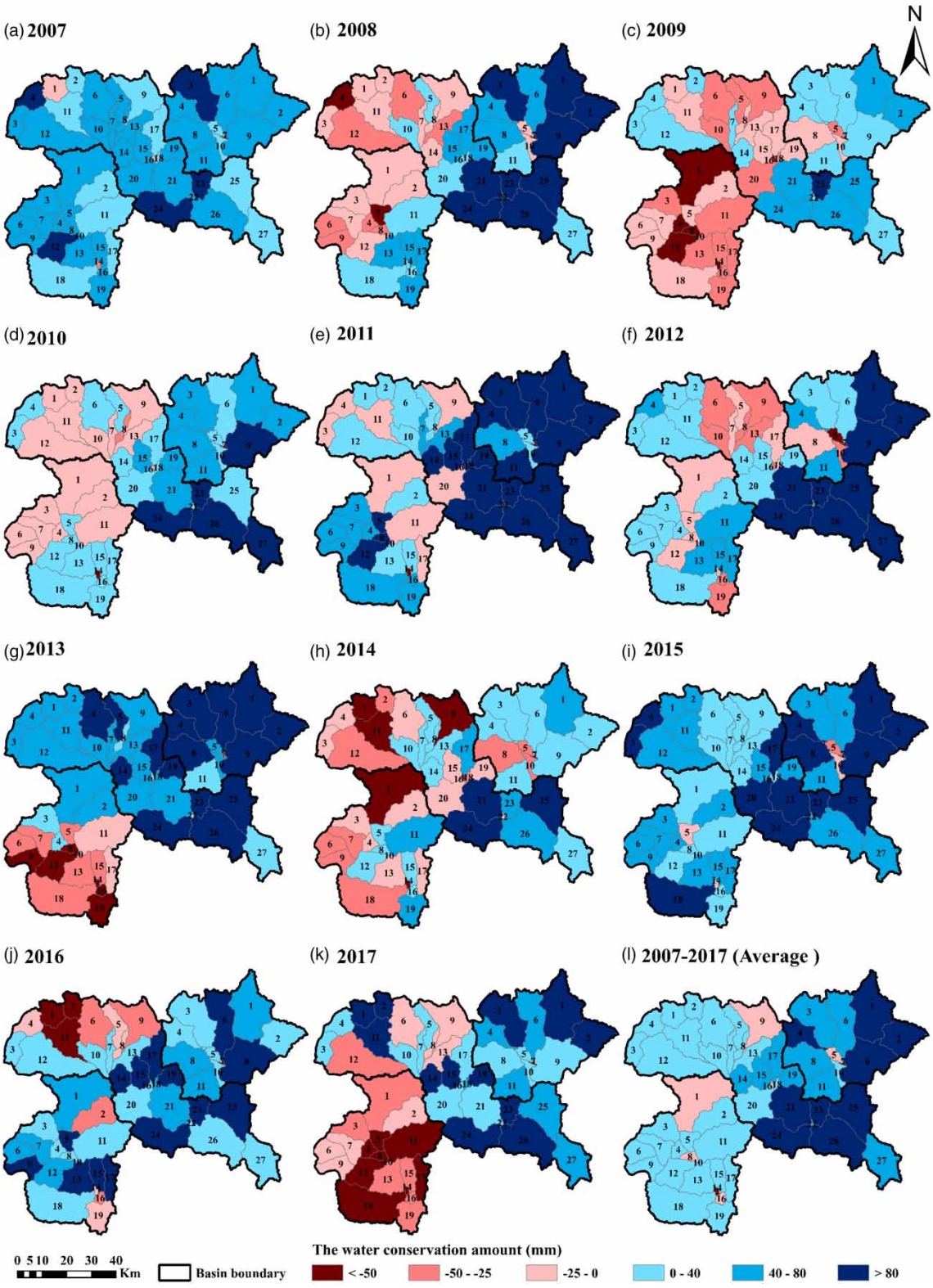

Figure 3 | Spatial distribution map of annual WCA from 2007 to 2017. (The numerical sequence number represents the order of the sub-basin).

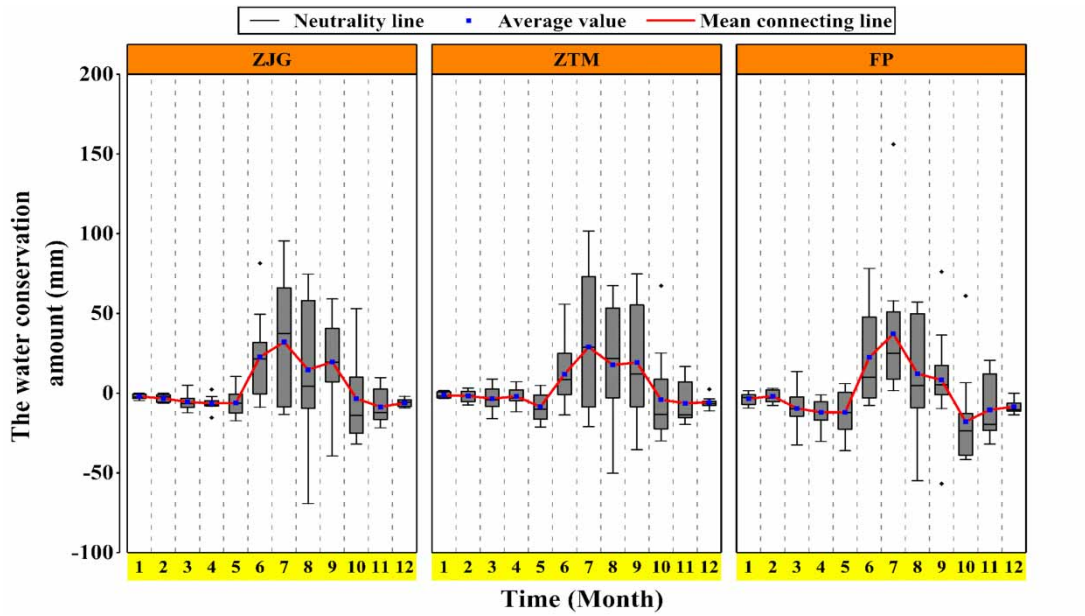

Figure 4 | Monthly variation of WCA in the three basins.

WCA appeared in sub-basins 6, 7 (Figure 5(k)). In October, the FP basin was mainly the high negative value regions of WCA, and only the upstream No. 1 and 2 sub-basins were the moderate negative value regions of WCA (Figure 5(j)). The WCA in the ZTM basin was the lowest in May, with a value of −8.56 mm. At this time, the ZTM basin was mainly the moderate and low negative value region of WCA (Figure 5(e)).

Analysis of factors affecting the change of WCA

Analysis of factors affecting the time change of WCA

We used SPSS 22.0 to perform multiple linear regression to obtain the relationship and significance between the interannual variation of WCA and precipitation, potential evapotranspiration, and population density.

It can be seen from the R^2 in Table 3 that the fitting equation can reflect the relevant factor information very well, indicating that there was an excellent linear relationship between WCA and the influencing factors. The WCA in the ZJG and ZTM basins showed a significant positive correlation with precipitation ($p < 0.05$), while the WCA in the FP basin showed a significant negative correlation with potential evapotranspiration ($p < 0.05$).

It can be seen from R^2 in Table 4 that there was an excellent linear relationship between WCA and influencing factors, and the R^2 of the monthly scale was greater than the R^2 of the annual scale in each basin. The WCA in ZJG and FP basins was significantly positively correlated with precipitation ($P < 0.05$). There was a significant positive correlation between WCA and precipitation in the ZTM basin ($P < 0.05$) and a significant negative correlation between WCA and potential evapotranspiration ($P < 0.05$).

Analysis of factors affecting the spatial pattern of WCA

The factor detector analysis results showed (Table 5) that the three most prominent factors affecting the spatial distribution of WCA in the ZJG basin were: potential evapotranspiration ($q = 0.813$) > precipitation ($q = 0.783$) > soil type ($q = 0.306$). The three most prominent factors affecting the spatial distribution of WCA in the ZTM basin were: precipitation ($q = 0.891$)> potential evapotranspiration ($q = 0.817$) > altitude ($q = 0.506$). Besides, soil type also has a more significant impact on the spatial distribution of the ZTM basin, with a q value of 0.461; The three most prominent factors affecting the spatial distribution of WCA in the FP basin were: precipitation ($q = 0.730$) > potential evapotranspiration ($q = 0.542$) > altitude ($q = 0.191$).

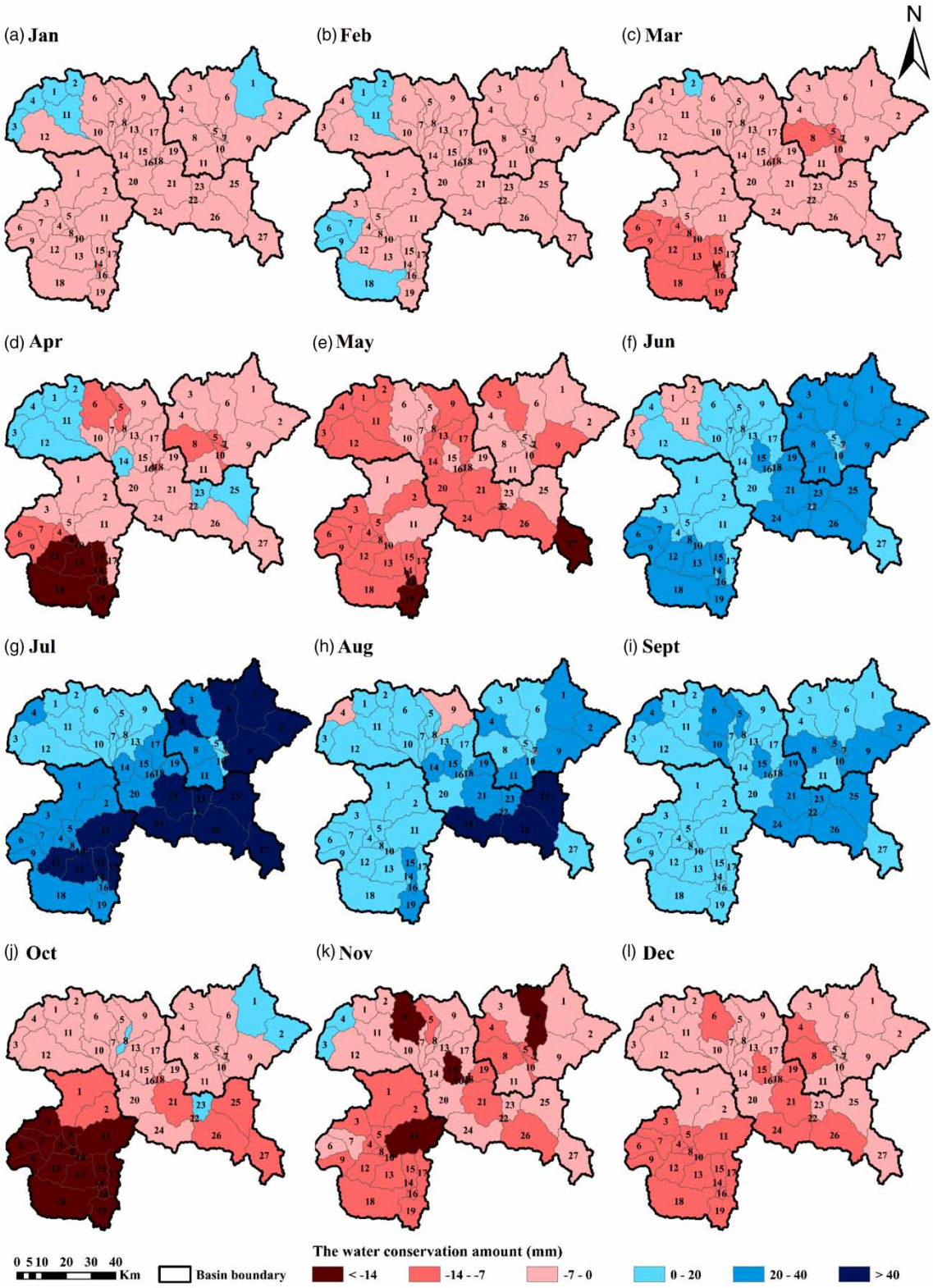

Figure 5 | Monthly spatial distribution of WCA for the three basins. (The numerical sequence number represents the order of the sub-basin).

Table 3 | Analysis of influencing factors of inter-annual variation of WCA

Basin	Impact factor	Beta	R^2	Significance	VIF
ZJG	Precipitation	0.867	0.711	0.006	1.223
	Potential evapotranspiration	0.016		0.945	1.238
	Population density	0.084		0.770	1.112
ZTM	Precipitation	0.854	0.601	0.019	1.402
	Potential evapotranspiration	0.193		0.515	1.386
	Population density	−0.039		0.876	1.014
FP	Precipitation	0.08	0.625	0.801	1.728
	Potential evapotranspiration	−0.743		0.044	1.715
	Population density	0.430		0.176	1.521

Table 4 | Analysis of influencing factors on the inter-monthly variation of WCA

Basin	Impact factor	Beta	R^2	Significance	VIF
ZJG	Precipitation	1.087	0.918	0.000	1.873
	Potential evapotranspiration	−0.206		0.179	1.873
ZTM	Precipitation	1.160	0.913	0.000	1.949
	Potential evapotranspiration	−0.337		0.036	1.949
FP	Precipitation	1.050	0.805	0.000	1.785
	Potential evapotranspiration	−0.264		0.212	1.785

Table 5 | Single factor detector in ZJG, ZTM and FP basins

		Climate		Topography		Underlying surface		Social and Economic	
Basin	Sample capacity	Precipitation	Potential evapotranspiration	Altitude	Slope	Soil type	Land use	GDP	Population density
ZJG	6,739	0.783	0.813	0.113	0.003	0.306	0.020	0.016	0.004
ZTM	13,193	0.891	0.817	0.506	0.044	0.461	0.051	0.047	0.024
FP	8,273	0.730	0.542	0.191	0.001	0.162	0.034	0.039	0.062

The analysis results of the interaction detector show that the top three interaction factors of explanatory power in the ZJG basin were PRE ∩ PET (q = 0.953), PET ∩ Soil type (p = 0.932), PRE ∩ Soil type (q = 0.853) (Table 6); the top three interaction factors of explanatory power in the ZTM basin were PRE ∩ PET (q = 0.987) > PET ∩ Soil type (p = 0.944) > PRE ∩ Soil type (q = 0.935) (Table 7); the top three interaction factors of explanatory power in the FP basin were PRE ∩ PET (q = 0.993) > PRE ∩ Soil type (p = 0.860) > PRE ∩ Altitude (q = 0.793) (Table 8). (PRE:Precipitation; PET:Potential evapotranspiration).

DISCUSSION

Our results show that precipitation, soil type, potential evapotranspiration, altitude, and their interactions are the main reasons for the differences in the spatial distribution of WCA in the three basins of the study area.

When the precipitation exceeds the interception, depression detention, and infiltration of the underlying surface, surface runoff will occur (Tang *et al.* 2019). Regardless of whether it is a runoff generation under saturated conditions or a runoff resulted from excess rain, the

Table 6 | Interaction detector in ZJG basin (q value)

	PRE	PET	Altitude	Slope	Soil type	Land use	GDP	PD
PRE	0.783							
PET	0.953	0.813						
Altitude	0.835	0.830	0.113					
Slope	0.790	0.832	0.163	0.003				
Soil type	0.853	0.932	0.403	0.322	0.306			
Land use	0.798	0.857	0.215	0.037	0.345	0.020		
GDP	0.811	0.835	0.153	0.050	0.360	0.064	0.016	
PD	0.796	0.872	0.188	0.016	0.332	0.040	0.081	0.004

(PRE: Precipitation; PET: Potential evapotranspiration; PD: Population density).

Table 7 | Interaction detector in ZTM basin (q value)

	PRE	PET	Altitude	Slope	Soil type	Land use	GDP	PD
PRE	0.891							
PET	0.987	0.817						
Altitude	0.906	0.864	0.506					
Slope	0.898	0.834	0.605	0.044				
Soil type	0.935	0.944	0.805	0.483	0.461			
Land use	0.898	0.834	0.614	0.073	0.492	0.051		
GDP	0.896	0.824	0.540	0.105	0.534	0.111	0.047	
PD	0.898	0.831	0.566	0.083	0.501	0.094	0.075	0.024

(PRE: Precipitation; PET: Potential evapotranspiration; PD: Population density).

Table 8 | Interaction detector in FP basin (q value)

	PRE	PET	Altitude	Slope	Soil type	Land use	GDP	PD
PRE	0.730							
PET	0.993	0.542						
Altitude	0.793	0.692	0.191					
Slope	0.749	0.551	0.215	0.001				
Soil type	0.860	0.738	0.477	0.185	0.162			
Land use	0.787	0.561	0.286	0.039	0.211	0.034		
GDP	0.733	0.568	0.209	0.049	0.195	0.082	0.039	
PD	0.753	0.586	0.210	0.071	0.238	0.117	0.086	0.062

(PRE: Precipitation; PET: Potential evapotranspiration; PD: Population density).

surface runoff increases with the increase in precipitation, which further affects the WCF (Jiang *et al.* 2018). Evapotranspiration is the main form of surface water consumption affected by multiple factors such as atmospheric temperature, water vapor pressure, wind speed, solar radiation, and underlying surface conditions (Maček *et al.* 2018; Liu *et al.* 2019). Soil evaporation and vegetation transpiration are the primary forms of basin

evapotranspiration, which together consume the water stored in the basin, and the amount of evapotranspiration directly affects the WCA of the basin (Li *et al.* 2016). Affected by various factors such as atmospheric circulation and topography, precipitation and evapotranspiration in mountainous areas have obvious spatial stratified heterogeneity, which affects the spatial distribution characteristics of WCA (Zhu *et al.* 2012).

The soil layer is the main body of terrestrial ecosystems for water conservation (Bormann 2012). Previous studies have shown that the smaller the soil bulk density, the relatively loose and porous the soil, the larger the capillary porosity, the faster the water seepage, making the soil layer store more water, thereby improving the soil's water conservation capacity (Bauer *et al.* 2014). As an inhomogeneous and changing space-time continuum, soil resources are affected by natural factors such as soil parent materials, topography, precipitation, and human activities, and have a high spatial stratified heterogeneity (Zhang *et al.* 2012; Reza *et al.* 2015). Besides, different soil types have different physical and chemical properties such as texture, organic matter, and soil bulk density. Therefore, the spatial stratified heterogeneity of soil significantly affects the spatial distribution of WCA.

As a natural geographic change, the altitude gradient directly affects the vertical distribution of precipitation and evapotranspiration, which affects the physical and chemical properties of soil, soil water and heat conditions, vegetation distribution, and vegetation density. It ultimately results in gradient changes in WCF (Li *et al.* 2012). The upstream of Xiong'an New Area is located in a mountainous area, and the topography in the area is very undulating. The elevation of different regions is quite different in this area, which leads to the difference in the spatial distribution of WCA.

CONCLUSIONS

The SWAT model constructed in the three catchments upstream of the Xiong'an New Area has high accuracy, and can reasonably reflect the hydrological cycle process on the annual and monthly scales of the three basins, and provides a tool for the accurate estimation of the basin WCA. On an annual scale, during the study period, the inter-annual changes in WCA in the ZJG, ZTM, and FP basins were large, and the average multi-year WCA was 47.59 mm, 44.59 mm, and 4.55 mm, respectively. The annual WCA of the ZTM basin was always positive. The WCA of the ZJG and FP basins showed negative values in 2009, 2014, and in 2009, 2013, 2014, respectively. Spatially, the WCA in parts of the upstream of the ZJG basin, parts of the middle and upper reaches of the ZTM basin, and the FP basin has undergone a positive and negative conversion between years. The areas where the WCA has not changed in positive or negative values also have changes in the high and low values of the WCA. On a monthly scale, there are apparent monthly differences in WCA in the ZJG, ZTM, and FP basins. The WCA of the rainy season months (June-September) are all positive, and the WCA of the non-rainy months (May-October) are all negative. Spatially, each sub-basin of the ZJG, ZTM, and FP basins has a positive and negative value conversion of WCA between the rainy season and the non-rainy season. Precipitation, evapotranspiration, and their combined effects are the main factors leading to the temporal changes and spatial pattern of WCA in the study area.

During the construction and operation management of the Xiong'an New Area, climate factors should be fully considered, and the urban functional layout and construction standards of significant infrastructure should be scientifically designed to reduce the adverse effects of climate change under the background of global warming.

ACKNOWLEDGEMENTS

This research was funded by the National Natural Science Foundation of China (No. 41877170), National Key Research and Development Program of China (No. 2018YFC0406501-02) and Hebei Province Key Research and Development Program of China (No. 20324203D and No. 20536001D). This work is supported by CFERN & BEIJING TECHNO SOLUTIONS Award Funds on excellent academic achievements.

DATA AVAILABILITY STATEMENT

Data cannot be made publicly available; readers should contact the corresponding author for details.

REFERENCES

Bauer, T., Strauss, P. & Murer, E. 2014 A photogrammetric method for calculating soil bulk density§. *Journal of Plant Nutrition and Soil Science* **177** (4), 496–499.

Bormann, H. 2012 Assessing the soil texture-specific sensitivity of simulated soil moisture to projected climate change by SVAT modelling. *Geoderma* **185–186**, 73–83.

Cao, Y., Zhang, J., Yang, M., Lei, X., Guo, B., Yang, L., Zeng, Z. & Qu, J. 2018 Application of SWAT model with CMADS data to estimate hydrological elements and parameter uncertainty based on SUFI-2 algorithm in the Lijiang River Basin, China. *Water* **10** (6).

Cao, W., Wu, D., Huang, L. & Liu, L. 2020 Spatial and temporal variations and significance identification of ecosystem services in the Sanjiangyuan National Park, China. *Scientific Reports* **10** (1), 6151.

Cong, W., Sun, X., Guo, H. & Shan, R. 2020 Comparison of the SWAT and InVEST models to determine hydrological ecosystem service spatial patterns, priorities and trade-offs in a complex basin. *Ecological Indicators* **112**, 106089.

Cui, H., Xiao, W., Zhou, Y., Hou, B., Lu, F. & Pei, M. 2019 Spatial and temporal variations in vegetation cover and responses to climatic variables in the Daqing River Basin, North China. *Journal of Coastal Research* **93**, 450.

Davies-Barnard, T., Valdes, P. J., Jones, C. D. & Singarayer, J. S. 2014 Sensitivity of a coupled climate model to canopy interception capacity. *Climate Dynamics* **42** (7–8), 1715–1732.

Ding, C., Zhang, H., Li, X., Li, W. & Gao, Y. 2017 Quantitative assessment of water conservation function of the natural spruce forest in the central Tianshang Mountains: a case study of the Urumqi River Basin. *Acta Ecologica Sinica* **37** (11), 3733–3743.

Han, E., Merwade, V. & Heathman, G. C. 2012 Implementation of surface soil moisture data assimilation with watershed scale distributed hydrological model. *Journal of Hydrology* **416–417**, 98–117.

Immerzeel, W. W., Lutz, A. F., Andrade, M., Bahl, A., Biemans, H., Bolch, T., Hyde, S., Brumby, S., Davies, B. J., Elmore, A. C., Emmer, A., Feng, M., Fernandez, A., Haritashya, U., Kargel, J. S., Koppes, M., Kraaijenbrink, P. D. A., Kulkarni, A. V., Mayewski, P. A., Nepal, S., Pacheco, P., Painter, T. H., Pellicciotti, F., Rajaram, H., Rupper, S., Sinisalo, A., Shrestha, A. B., Viviroli, D., Wada, Y., Xiao, C., Yao, T. & Baillie, J. E. M. 2020 Importance and vulnerability of the world's water towers. *Nature* **577** (7790), 364–369.

Jiang, J., Wu, Y., Wang, X., Xu, L. & Fan, H. 2018 Identify the influencing paths of precipitation and soil water storage on runoff: an example from Xinjiang River Basin, Poyang Lake, China. *Water Supply* **18** (5), 1598–1605.

Jin-Feng, W., Christakos, G. & Mao-Gui, H. 2009 Modeling spatial means of surfaces with stratified nonhomogeneity. *IEEE Transactions on Geoscience and Remote Sensing* **47** (12), 4167–4174.

Kan, G., He, X., Ding, L., Li, J., Liang, K. & Hong, Y. 2017 Study on applicability of conceptual hydrological models for flood forecasting in humid, semi-humid semi-arid and arid basins in China. *Water* **9** (10).

Khatun, S., Sahana, M., Jain, S. K. & Jain, N. 2018 Simulation of surface runoff using semi distributed hydrological model for a part of Satluj Basin: parameterization and global sensitivity analysis using SWAT CUP. *Modeling Earth Systems and Environment* **4** (3), 1111–1124.

Kurihara, M., Onda, Y., Kato, H., Loffredo, N., Yasutaka, T. & Coppin, F. 2018 Radiocesium migration in the litter layer of different forest types in Fukushima, Japan. *Journal of Environmental Radioactivity* **187**, 81–89.

Li, Z., He, Y., Theakstone, W. H., Wang, X., Zhang, W., Cao, W., Du, J., Xin, H. & Chang, L. 2012 Altitude dependency of trends of daily climate extremes in southwestern China, 1961–2008. *Journal of Geographical Sciences* **22** (3), 416–430.

Li, X., Li, Y., Zhang, Q. & Xu, X. 2016 Evaluating the influence of water table depth on transpiration of two vegetation communities in a lake floodplain wetland. *Hydrology Research* **47** (S1), 293–312.

Liu, L., Cao, W. & Shao, Q. 2016 Water conservation function of forest ecosystem in the southern and borthern pan river watershed. *Scientia Geographica Sinica* **36** (4), 603–611.

Liu, Y. J., Chen, J. & Pan, T. 2019 Analysis of changes in reference evapotranspiration, pan evaporation, and actual evapotranspiration and their influencing factors in the north China plain during 1998–2005. *Earth and Space Science* **6** (8), 1366–1377.

Luo, Y., Lu, Y., Fu, B., Zhang, Q., Li, T., Hu, W. & Comber, A. 2019 Half century change of interactions among ecosystem services driven by ecological restoration: quantification and policy implications at a watershed scale in the Chinese Loess Plateau. *Science of the Total Environment* **651** (Pt 2), 2546–2557.

Maček, U., Bezak, N. & Šraj, M. 2018 Reference evapotranspiration changes in Slovenia, Europe. *Agricultural and Forest Meteorology* **260–261**, 183–192.

Moriasi, D. N., Arnold, J. G., Van Liew, M. W., Bingner, R. L., Harmel, R. D. & Veith, T. L. 2007 Model evaluation guidelines for systematic quantification of accuracy in watershed simulations. *Transactions of the ASABE* **50**, 885–900.

Nash, J. E. & Sutcliffe, J. V. 1970 River flow forecasting through conceptual models part I – A discussion of principles. *Journal of Hydrology* **10**, 282–290.

Návar, J. 2017 Fitting rainfall interception models to forest ecosystems of Mexico. *Journal of Hydrology* **548**, 458–470.

Reza, S. K., Nayak, D. C., Chattopadhyay, T., Mukhopadhyay, S., Singh, S. K. & Srinivasan, R. 2015 Spatial distribution of soil physical properties of alluvial soils: a geostatistical approach. *Archives of Agronomy and Soil Science* **62** (7), 972–981.

Scordo, F., Lavender, T., Seitz, C., Perillo, V., Rusak, J., Piccolo, M. & Perillo, G. 2018 Modeling water yield: assessing the role of site and region-specific attributes in determining model performance of the InVEST seasonal water yield model. *Water* **10** (11), 1496.

Tang, Y., Tang, Q., Wang, Z., Chiew, F. H. S., Zhang, X. & Xiao, H. 2019 Different precipitation elasticity of runoff for precipitation increase and decrease at watershed scale. *Journal of Geophysical Research: Atmospheres* **124** (22), 11932–11943.

Todorova, Y., Lincheva, S., Yotinov, I. & Topalova, Y. 2016 Contamination and ecological risk assessment of long-term polluted sediments with heavy metals in small hydropower cascade. *Water Resources Management* **30** (12), 4171–4184.

van Griensven, A., Meixner, T., Grunwald, S., Bishop, T., Diluzio, M. & Srinivasan, R. 2006 A global sensitivity analysis tool for the parameters of multi-variable catchment models. *Journal of Hydrology* **324** (1–4), 10–23.

Wang, J.-F. & Hu, Y. 2012 Environmental health risk detection with GeogDetector. *Environmental Modelling & Software* **33**, 114–115.

Wang, J. F., Li, X. H., Christakos, G., Liao, Y. L., Zhang, T., Gu, X. & Zheng, X. Y. 2010 Geographical detectors-based health risk assessment and its application in the neural tube defects study of the Heshun Region, China. *International Journal of Geographical Information Science* **24** (1), 107–127.

Wang, X., Shen, H., Li, X. & Jing, F. 2013 Concepts,processes and quantification methods of the forest water conservation at the multiple scales. *Acta Ecologica Sinica* **33** (4), 1019–1030.

Wang, Z., Cao, J. & Yang, H. 2021 Multi-time scale evaluation of forest water conservation function in the semiarid mountains area. *Forests* **12** (2).

Xu, J., Ji, G., Meadows, M. E., Chen, R. & Yang, X. 2020 Modelling water yield with the InVEST model in a data scarce region of northwest China. *Water Supply* **20** (3), 1035–1045.

Yang, Q., Zhang, X., Almendinger, J. E., Huang, M., Leng, G., Zhou, Y., Zhao, K., Asrar, G. R., Li, X. & Qiu, J. 2018 Improving the SWAT forest module for enhancing water resource projections: a case study in the St. Croix River Basin. *Hydrological Processes* **33** (5), 864–875.

Zhang, T., Zhang, L., Jiang, L., Zhao, S., Zhao, T. & Li, Y. 2012 Effects of spatial distribution of soil parameters on soil moisture retrieval from passive microwave remote sensing. *Science China Earth Sciences* **55** (8), 1313–1322.

Zhao, G., Zhou, H., Liu, X., Li, K., Zhang, P., Wen, W. & Yu, Y. 2012 PHAHs in 14 principal river sediments from Hai River basin, China. *Science of the Total Environment* **427–428**, 139–145.

Zhou, G., Wei, X., Luo, Y., Zhang, M., Li, Y., Qiao, Y., Liu, H. & Wang, C. 2010 Forest recovery and river discharge at the regional scale of Guangdong Province, China. *Water Resources Research* **46** (9), W09503.

Zhu, G., He, Y., Pu, T., Wang, X., Jia, W., Li, Z. & Xin, H. 2012 Spatial distribution and temporal trends in potential evapotranspiration over Hengduan Mountains region from 1960 to 2009. *Journal of Geographical Sciences* **22** (1), 71–85.

Zuo, D., Xu, Z., Yao, W., Jin, S., Xiao, P. & Ran, D. 2016 Assessing the effects of changes in land use and climate on runoff and sediment yields from a watershed in the Loess Plateau of China. *Science of the Total Environment* **544**, 238–250.

First received 24 October 2020; accepted in revised form 20 April 2021. Available online 4 May 2021